Chemical Science

EDGE ARTICLE

View Article Online
View Journal | View Issue

Cite this: *Chem. Sci.*, 2019, **10**, 1644

All publication charges for this article have been paid for by the Royal Society of Chemistry

Color-tunable lanthanide metal–organic framework gels†

Fei Chen,[a] Yong-Mei Wang,[a] Weiwei Guo [a] and Xue-Bo Yin *[ab]

Received 24th October 2018
Accepted 28th November 2018

DOI: 10.1039/c8sc04732d

rsc.li/chemical-science

Fluorescence significantly improves the performance of gels. Various strategies, such as embedment and crosslinking, have been used to integrate extrinsic luminophores into gel systems, but the procedures are usually complex. Herein, for the first time, we report gels with intrinsic and tunable emission color prepared with 5-boronoisophthalic acid (5-bop) and Eu^{3+}, Tb^{3+}, and/or Dy^{3+} similar to the procedure for the preparation of metal–organic frameworks (MOFs). The single-metal gels exhibit intrinsic trichromatic fluorescence, due to which full-color emissions are readily obtained by tuning the type and/or ratio of Ln^{3+} ions to prepare mixed-metal gels. The emission is governed by an antenna effect and is thus excited with single-wavelength at 275 nm. The nucleation-growth mechanism reveals that the Ln^{3+} ions and 5-bop produce separated layers, which then grow anisotropically to form nanoribbons by high coordinated valence of Ln^{3+} ions and biased carboxyl distribution as well as steric hindrance and hydrogen bonds of the boric acid group in 5-bop. The nanoribbons entangle together to generate chemical-physical hybrid gels. To the best of our knowledge, this is the first example of gels with inherent and tunable emission color. Due to their optical and viscoelastic properties, the gels have numerous potential applications such as tunable emission and multi-target detection.

Introduction

Gels are solid-like materials, where the solvent molecules are immobilized in the network of gelators.[1,2] Viscoelastic properties are mainly used to respond to external stimuli[3] such as heat, pH, light, and mechanical force with the gels as biomaterials,[4–6] stimuli-responsive materials,[7–10] sensors,[11,12] and host–guest systems.[13–15] Ever-increasing applications are associated with the luminescent gels as fluorescence significantly improves the performance of the gel materials.[4,16,17] Fluorogenic probes were inserted in the monomer that contained glucose-recognition sites, spacers, and polymerization sites to prepare a glucose-response emissive gel to monitor glucose concentration *in vivo*.[4] Three fluorescent dyes were crosslinked to bovine serum albumin to form a dual-emission gel for the ratiometric fluorescence sensing of Fe^{3+} ions.[16] Eu^{3+}, Tb^{3+}, and carbon dots were integrated into polyacrylamide/poly(acrylic acid) hybrid gels as multifunctional materials for chemical sensing.[17]

Although a complex procedure is required to introduce extrinsic luminophores,[4,16,17] fluorescent gels are still less reported. An alternative assembly strategy, in combination with unconventional precursors, is thus essential to establish gels with intrinsic emission. Metal–organic frameworks (MOFs) are the assembly between metal ions (or clusters) and organic ligands.[18] Some MOF gels were reported,[19–24] but the formed MOF nanoparticles coordinated with mismatched growth and gelation.[19] Therefore, the so-called "gels" were still MOFs but in amorphous state.[19–24] The other strategy is tantamount to embed nanoscale MOFs into the polymer matrix.[25,26] Can the assembly procedure used for the formation of MOFs be employed in the preparation of gels? Similar to low-molecular-weight gels,[1,2] if metal ions and organic ligands grow anisotropically to constitute flexible fibers or ribbons, fibers or ribbons may entangle together to form valid MOF gels.

Herein, we report that the ligand with biased carboxyl distribution, such as isophthalic acid (ISP) derivative, is selected to form a ribbon-like structure, followed by gelation upon the entanglement of nanoribbons. The introduction of a boric acid group in ISP improves the anisotropic growth through steric hindrance and hydrogen bonds (Fig. 1A). Metal ions with high coordination valences also enhance the anisotropic growth.[27,28] Therefore, a series of emissive MOF gels are prepared successfully with 5-boronoisophthalic acid (5-bop) as the ligand and single- or mixed-Ln^{3+} ions, including Eu^{3+}, Tb^{3+}, and Dy^{3+}, as metal nodes for the first time. Single-metal MOFs exhibit trichromatic fluorescence; thus, full-color emissions are readily obtained by tuning the types and/or ratios of Ln^{3+} ions to prepare mixed-metal MOF gels (Fig. 1A). Tb^{3+} and Dy^{3+} ions

[a]*State Key Laboratory of Medicinal Chemical Biology, Tianjin Key Laboratory of Biosensing and Molecular Recognition, College of Chemistry, Nankai University, Tianjin, 300071, China. E-mail: xbyin@nankai.edu.cn; Fax: +86-22-23503034*

[b]*Collaborative Innovation Center of Chemical Science and Engineering (Tianjin), Nankai University, Tianjin, 300071, China*

† Electronic supplementary information (ESI) available: All experimental details, crystallographic data collection and refinement statistics, details of chemical synthesis, additional figures and tables. See DOI: 10.1039/c8sc04732d

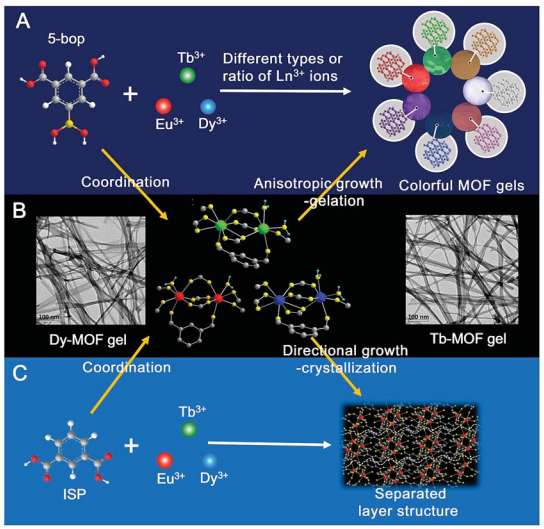

Fig. 1 (A) The selection of different types and ratios of Ln^{3+} ions for the formation of MOF gels with different colors. (B) The formation of Tb- and Dy-MOF gels because of their different coordination environments compared to that of Eu^{3+}. (C) Separated layer structure revealed from single crystal results for the formation of nanoribbons, which entangle together to form MOF gels.

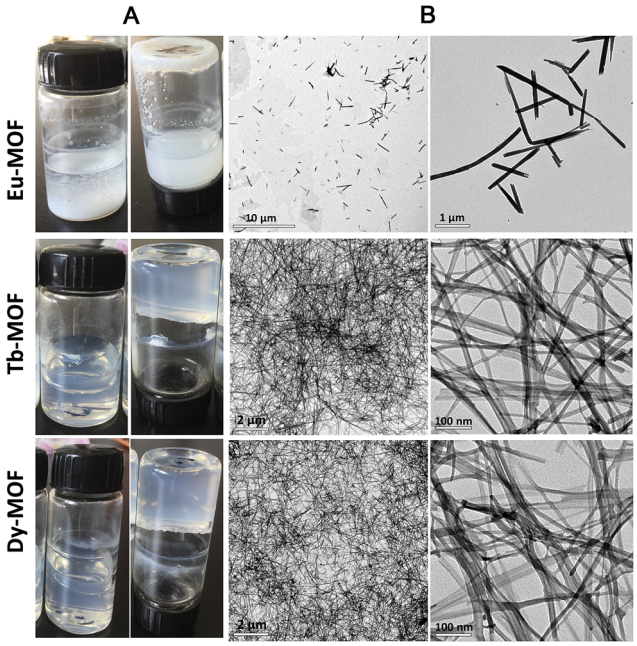

Fig. 2 (A) Photographs and (B) transmission electron microscopy (TEM) images with different amplification of Eu-MOFs, Tb-MOFs, and Dy-MOFs. The MOFs were prepared with 0.1 mmol 5-bop as the ligand and 0.1 mmol Eu^{3+}, Tb^{3+}, or Dy^{3+} ions as metal nodes in 10 mL DMF/H_2O under 120 °C under atmospheric pressure.

form MOF gels easily with 5-bop as the ligand because their coordination environments are different from that of Eu^{3+} ions (Fig. 1B). However, mixed-metal MOF gels are easily prepared to obtain gels with different colors. Formation mechanism study indicates that the precursors form separated layers (Fig. 1C), which grow anisotropically to form nanoribbons by the high coordination valence of Ln^{3+} ions and biased carboxyl distribution as well as steric hindrance and hydrogen bonds of the boric acid group. Nanoribbons entangle together to form MOF gels. Nanoribbons are formed through chemical bonding between 5-bop and metal ions similar to chemical gels; the nanoribbons entangle through non-covalent interaction, which is the essential property of physical gels. Chemical/physical hybrid gels with intrinsic fluorescence emission were thus reported.

Results and discussion

Preparation and properties of single-metal MOFs

Ln-MOFs were prepared with Eu^{3+}, Tb^{3+}, and Dy^{3+} as metal nodes and 5-bop as the ligand hydrothermally.[29] Eu-MOFs existed as precipitates, whereas Tb-MOFs and Dy-MOFs became uniform semi-transparent gel-like products after reaction for 12 h (Fig. 2A). The difference was revealed with their different morphologies, as observed from the TEM images (Fig. 2B). Eu-MOFs formed nanorods with breadth of 100 nm and length at the micrometer level. Tb- and Dy-MOFs assembled into nanoribbons with breadth of 20 nm and length well above 10 μm with an aspect ratio higher than 500. The nanoribbons were flexible enough and therefore entangled and interlaced with each other to form MOF gels. The different structures were also revealed from their SEM images. Tb- and Dy-MOFs gels were formed through the entanglement of nanoribbons, and the rod-like structure of Eu-MOFs was observed (Fig. S1†).

Rheological measurements confirmed the viscoelastic properties of Tb- and Dy-MOF gels. The linear viscoelastic region of the MOF gel systems was delineated by a strain amplitude sweep (Fig. 3A and C). The results in Fig. 3B and D depict the frequency sweep results of the gel systems, where the value of storage modulus G' is markedly higher than that of the loss modulus G'' throughout the test region (ω = 0.1–100 rad s^{-1}). Strain amplitude sweep measurements show that both the G' and G'' moduli remain constant in a certain range of strain. The G'' modulus plateau is at a higher value than that of G', illustrating the degradation of the gel structure. High-yield strain (γ value) suggests that the gels are strongly damage resistant. The gel properties of Tb- and Dy-MOFs were thus confirmed.

The characteristic emission peaks of Ln^{3+} ions were clearly observed from the fluorescence profiles of Eu-, Tb-, and Dy-MOFs (Fig. 3E–G);[30] interestingly, their emissions show the trichromatic colors red, green, and blue, respectively (Fig. 3H). Therefore, full-color emissions are easily obtained according to the trichromatic theory. The emission is governed by the antenna effect, as schematized in Fig. 3I.[31] The ligand 5-bop is excited to its singlet state (S_1, Table S1†) and then transfers to its triplet state (T_1) through intersystem crossing.[31] Ln^{3+} ions are then sensitized by the triplet state to excite their emissions. The emissions are observed from Eu- and Tb-MOFs as procedures "a" and "b" in Fig. 3H. Competing energy transfer occurs in Dy-MOF gels because the T_1 energy of 5-bop is close to that of $^4F_{9/2}$ of Dy^{3+} for low radiative energy transition. Instead, nonradiative

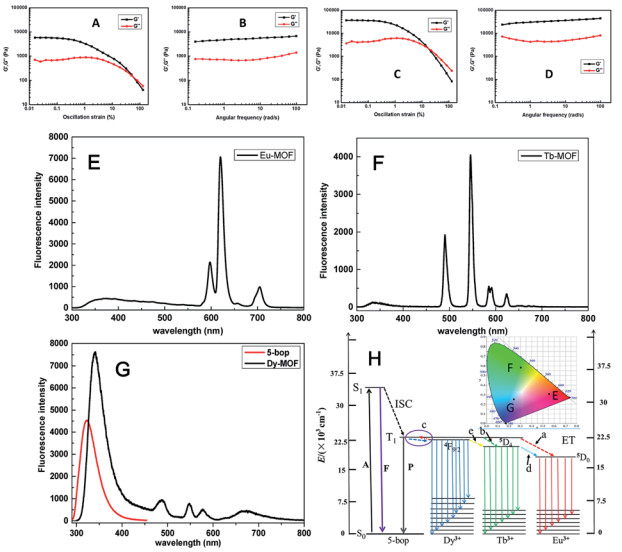

Fig. 3 Viscoelastic properties of (A, B) Tb-MOF and (C, D) Dy-MOF gels. Fluorescence spectra of (E) Eu-MOFs, (F) Tb-MOFs, and (G) Dy-MOFs and 5-bop under single-wavelength excitation at 275 nm. (H) Antenna effect emission mechanism of Ln-MOFs. The "a", "b", and "c" procedures represent the energy transfer from T1 of 5-bop to Eu^{3+}, Tb^{3+}, and Dy^{3+}. The "d" and "e" procedures illustrate the energy transfer from the excited state of Tb^{3+} to Eu^{3+} and that from Dy^{3+} to Tb^{3+}. Inset: CIE chromaticity coordinates of the emissions from (E) Eu-MOFs, (F) Tb-MOFs, and (G) Dy-MOFs. Abbreviations: "A", absorption at 275 nm; "F", fluorescence at 366 nm; "P", phosphorescence; ISC, intersystem crossing; ET, energy transfer; S1, singlet; and T1, triplet.

transition from $^4F_{9/2}$ of Dy^{3+} to T_1 of 5-bop occurs easily. Thus, the blue emission of Dy-MOF gels was partly due to 5-bop with the procedure "c" shown in Fig. 3H. The antenna effect governs the emission of MOFs; thus, single-wavelength excitation achieves all the emissions to facilitate their practical application.[32]

Formation mechanism of MOF gels

Tb^{3+} and Dy^{3+} are necessary for the formation of MOF gels. To validate the role of 5-bop, its counterpart, isophthalic acid (ISP), was selected as the ligand to prepare Ln-ISP MOFs. However, all the Ln^{3+} ions could not form Ln-ISP MOF gels (Fig. S2†). The addition of the boric group in the side chain of ISP altered the entropy, hydrogen bonds and steric hindrance of the ligand,[33] necessitating a favorable change for the formation of nanoribbons. Therefore, Tb^{3+} and Dy^{3+} must be used as the metal nodes, whereas 5-bop plays an important role in the formation of MOF gels.

Tb-MOFs with different reaction times were characterized to reveal the formation of the gels (Fig. S3†). The precursors were still transparent in the solution state at 1 h. After 2 h, the fluidity of the solution decreased considerably, and "non-flowing" gel property was observed at 3 h. The transparency of the gels decreased gradually as the reaction time increased from 3 to 12 h. TEM images revealed the structural change. After 1 h, the precursors formed irregular clusters (Fig. S4A†). Filiform products were observed at 1.5 h (Fig. S4B†). With increasing reaction time from 1.5 to 3 h, the content of filiform products increased, whereas the clusters decreased and disappeared (Fig. S4B–E†). After 6 h, nanoribbons were formed and they entangled to form MOF gels (Fig. S4F†). Moreover, high yield was achieved as almost all the precursors formed MOF gels, as revealed by the TEM images (Fig. S4F†).

The precursor concentration was tested. When the content of Tb^{3+} was lower than 0.2 mmol in 10 mL of DMF/H_2O, the MOF gel was formed in a normal manner (Fig. S5A†). Tb-MOFs became precipitates when the content was higher than 0.4 mmol. The morphology was clearly evident from their TEM images (Fig. S5B–E†). The nanoribbons of Tb-MOFs gradually became shorter and thicker with increasing Tb content. Moreover, the nanoribbons became rigid to prevent their entangling to form gels. Therefore, the formation of MOF gels was governed by the nucleation-growth mechanism. A rapid nucleation occurred under the initial period, whereas diluted solution yielded modest amounts of crystal nuclei, which then grew slowly to form long nanoribbons. The nanoribbons were flexible and entangled to constitute the gel. Aligned hydrogen bonds between the nanoribbons were present, resulting in the stability of the assembled MOF gels.

Single-crystal data can provide evidence of gel formation at the atomic level. Single-crystal MOFs were thus prepared with ISP as the ligand and Eu^{3+}, Tb^{3+}, or Dy^{3+} as the metal nodes. ISP-MOFs exhibit a monoclinic system with space group $P2_1/n$ or $P2_1/c$ (Tables S2–S4†). The fundamental building unit of Eu-ISP MOFs contains two non-equivalent Eu^{3+} ions, three deprotonated ISP molecules, and two H_2O molecules, with the formula $Eu_2(ISP)_3(H_2O)_2$. The H_2O molecules are coordinated to the two Eu^{3+} ions (Fig. 4A). Tb- and Dy-ISP MOFs show the same configuration with the formulae of $Tb_2(ISP)_3(H_2O)_2 \cdot H_2O$ and $Dy_4(ISP)_6(H_2O)_4 \cdot H_2O_2$, respectively. While two H_2O molecules are coordinated to single Tb^{3+} or Dy^{3+} ion, the third H_2O molecule exists in the channel (Fig. 4B and C). Tb1 and Dy1 are eight-coordinated, but Tb2, Dy2, Eu1, and Eu2 ions show seven-coordinated pentagonal bipyramidal geometry (Fig. 4A–C). Due to slight differences in the coordination environments between Eu^{3+} and Tb^{3+} or Dy^{3+}, Eu^{3+} ions cannot form MOF gels easily.

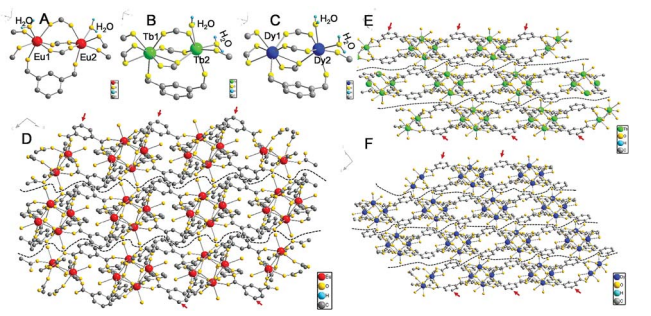

Fig. 4 Coordination environments of the two independent Ln^{3+} ions in the building unit of (A) Eu-ISP MOFs, (B) Tb-ISP MOFs, and (C) Dy-ISP MOFs. In (A), two H_2O molecules are coordinated to the two Eu^{3+} ions, whereas in (B) and (C), two H_2O molecules are coordinated to single Tb^{3+} or Dy^{3+} ion and the third H_2O molecule occupies the channel of MOFs. Discrete layer structure containing one-dimensional rod-like chains was revealed with dotted-lines and observed in (D) Eu-ISP MOFs, (E) Tb-ISP MOFs, and (F) Dy-ISP MOFs.

Eu1/Tb1/Dy1 and Eu2/Tb2/Dy2 atoms were arranged alternately and linked by discrete carboxylate groups of ISP to form 1D ribbon-like chains (Fig. 4D–F). Adjacent 1D chains connect with each other through the ligand to form a 2D layer structure. The high coordination valence of Ln^{3+} ions and biased carboxyl distribution in the ligands result in anisotropic growth to form a ribbon-like structure, as shown with arrows in Fig. 4D–F. If 5-bop is chosen as the ligand, the steric hindrance of the boric acid group enhances the anisotropic growth for the formation of nanoribbons. Interestingly, different layers are clearly separated without any chemical cross-linking, as illustrated with dotted lines in Fig. 4D–F. Thus, a layer structure was formed and also confirmed with high-resolution TEM images of Eu-ISP and Tb-ISP MOFs (Fig. S6†). The introduction of the boric acid group further led to the separation of the layers to form nanoribbons.

To prove the role of the boric acid unit in isophthalic acid for anisotropic growth, Ln-MOFs with [1,1′-biphenyl]-3,5-dicarboxylic acid as ligand were synthesized to confirm the effect of steric hindrance. 5-Hydroxyisophthalic acid and 5-aminoisophthalic acid were used as the ligands to verify the role of hydrogen bonds. All Ln-MOFs existed as precipitates (Fig. S7†). Their different morphologies were revealed from the TEM images (Fig. S8†). The morphology of Tb-MOFs was similar to that of Dy-MOFs but different to that of Eu-MOFs because of the different coordination environments of Ln^{3+} ions, as validated with the single-crystal results (Fig. 4). The gels could not form under the condition of single steric resistance taking the place of boric acid with the phenyl ring (Fig. S8A–C†); also, a ribbon-like structure was observed from Eu-[1,1′-biphenyl]-3,5-dicarboxylic acid-MOFs. Moreover, we did not obtain gels with single hydrogen bonds using amino and hydroxyl groups instead of boric acid (Fig. S8D–I†). However, an irregular slice layered structure was observed from Ln-MOFs prepared with 5-hydroxyisophthalic acid and 5-aminoisophthalic acid as the ligands. Therefore, the gel could be formed merely with the combination of steric hindrance and hydrogen bonds by the introduction of the boric acid group.

Powder XRD patterns of Eu-MOF, Tb-MOF gels, and Dy-MOF gels were recorded and compared with those of the single crystals of Eu-, Tb-, and Dy-ISP MOFs, respectively. Similar XRD patterns were observed for MOFs with 5-bop and ISP as the ligands (Fig. S9†). Thus, single-crystal data provided evidence for the formation of nanoribbons and the differences among Ln^{3+} ions as metal nodes. High-resolution TEM images reveal ribbons with thickness less than 20 nm (Fig. S8†). The length was greater than 10 μm and thus, the aspect ratio was higher than 500. The nanoribbons were formed through covalent bonds, which is a property of chemical gels;[7–10] no coordinative cross-linking was found between the nanoribbons (Fig. S6 and S10†) similar to that observed for supramolecular physical gels.[1,2] Therefore, our MOF gels were chemical/physical hybrid gels.

Mixed-metal MOF gels

Bimetallic or trimetallic ions were selected to prepare mixed-metal MOFs to obtain tunable emission color *via* different types and/or ratios of Ln^{3+} ions. Interestingly, all the mixed-metal precursors formed MOF gels successfully (Fig. 5A). TEM

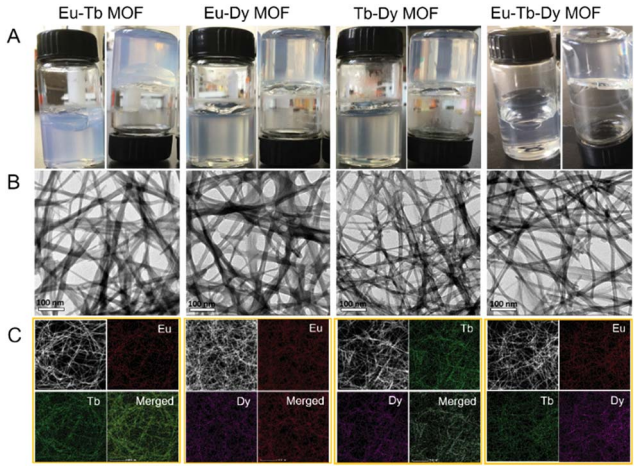

Fig. 5 (A) Photos and (B) TEM images of Eu–Tb, Eu–Dy, Tb–Dy, and Eu–Tb–Dy mixed-metal MOFs prepared with 5-bop as the ligand and 0.1 mmol mixed-metal precursors with metal ratios of 1 : 1 or 1 : 1 : 1 in 10 mL of DMF/H_2O at 120 °C under atmospheric pressure. (C) Scanning transmission electron microscopy images and energy-dispersive X-ray elemental mapping of the mixed-metal MOF gels.

and SEM images clearly revealed the nanoribbons and their entanglement to constitute gels (Fig. 5B and S11†). The peak at 1695 cm^{-1} was ascribed to the C=O stretching vibration ($\nu_{C=O}$) of 5-bop in the Fourier transform infrared spectra (Fig. S12†) but disappeared in the spectrum of MOF gels, suggesting that carboxylate groups coordinated to Ln^{3+} ions. The B–O absorption peak was observed at 1313 cm^{-1} for 5-bop and the mixed-metal MOF gels, indicating that the free boric acid site existed.

Element distribution of the mixed-metal MOF gels was first tested with scanning transmission electron microscopy (STEM) and energy-dispersive X-ray (EDX) elemental mapping. Each element was clearly observed in the images and distributed in the entire area of the MOF gels uniformly (Fig. 5C). Therefore, Eu, Tb, and Dy were successfully integrated into the mixed-metal MOF gels. The expected metals were observed from X-ray photoelectron spectroscopy (XPS) patterns, which also confirmed the formation of mixed-metal MOF gels (Fig. S13†). The mole ratios of Ln^{3+} ions were 1 : 0.80, 1 : 1.09, 1 : 1.21, and 1 : 0.94 : 0.91 in Eu–Tb, Eu–Dy, Tb–Dy, and Eu–Tb–Dy MOF gels, respectively, as revealed from the inductively coupled plasma-atomic emission spectrometry results (Table S5†). Rheological measurements confirmed that the moduli of the gels were a function of the applied angular frequency to disclose their gel properties (Fig. S14†). Therefore, mixed-metal MOF gels were formed by integrating different metal ions together.

The characteristic emissions of Ln^{3+} ions were well retained in the bimetallic MOF gels, but the intensity was markedly different from that shown in Fig. 3. The emission of Eu^{3+} ions in Eu–Tb MOF gels was retained, but the emission of Tb^{3+} ions was heavily suppressed (Fig. S15A†). We considered that part of the energy of $^5D_4$ of Tb^{3+} was transferred to $^5D_0$ of Eu^{3+} before radiative transition occurred with the "d" procedure shown in Fig. 3H.[32,34] The emission of Eu^{3+} ion was suppressed in Eu–Dy MOF gels (Fig. S15B†); $^4F_{9/2}$ of Dy^{3+} has much closer energy to T_1

of 5-bop than the $^5D_0$ state of Eu^{3+}, suggesting that energy transfers easily from 5-bop to Dy^{3+} ions as procedure "c" in Fig. 3H. Thus, blue emission was clearly observed, whereas that of the Eu^{3+} ions was heavily suppressed in Eu–Dy MOF gels.

The emission intensity of Tb^{3+} was retained in the Tb–Dy MOF gels, but the blue emission decreased clearly (Fig. S15C†). Energy was transferred from $^4F_{9/2}$ of Dy^{3+} to $^5D_4$ of Tb^{3+} with the "e" procedure shown in Fig. 3H. Fig. S15D† shows that the emissions of the mixed-metal MOF gels were not the simple summation from those of single-metal MOFs. Therefore, metal ions were integrated at the atomic level, enabling energy transfer between different Ln^{3+} ions. Isostructural MOF gels were easily prepared by tuning the types and ratios of Ln^{3+} ions for combined emissions, which show promise for colorful applications.

Tunable shape and emission color of MOF gels

White light-emitting materials attract much attention.[35–37] The emission color of MOF gels is easily tuned by the types and/or ratios of Ln^{3+} ions. When the ratio of Eu/Dy/Tb was chosen as 1 : 1 : 1 in the precursors, the emission was close to white with the CIE coordinate of (0.3788, 0.348) (Fig. 6A). White emission was clearly observed with the Ln^{3+} ion ratio of 1 : 1 : 2 with the CIE coordinate of (0.3108, 0.3402) (Fig. 6B). To explore their ability to simultaneously exhibit gel and emission properties, different MOF gels were poured into separate molds. The shapes of the molds were clearly outlined (Fig. 6C–F). Therefore, we report flexible MOF gels by the formation of flexible nanoribbons for the first time. Moreover, their colors were the same under sunlight, but their distinct and intrinsic emissions were observed under single-wavelength excitation at 275 nm (Fig. 6C–F).

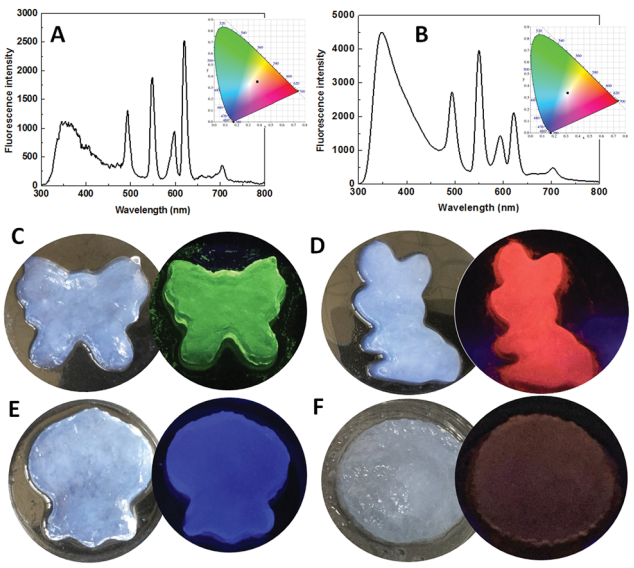

Fig. 6 Emission profiles of Eu–Tb–Dy MOF gels under the single-wavelength excitation at 275 nm with the Eu/Dy/Tb ratios of (A) 1 : 1 : 1 and (B) 1 : 1 : 2. Photographs of (C) Tb–Dy, (D) Eu–Tb, (E) Eu–Dy, and (F) Eu–Tb–Dy MOF gels with mixed-metal ratios of 1 : 1 or 1 : 1 : 1 under sunlight (left) and excitation at 275 nm (right).

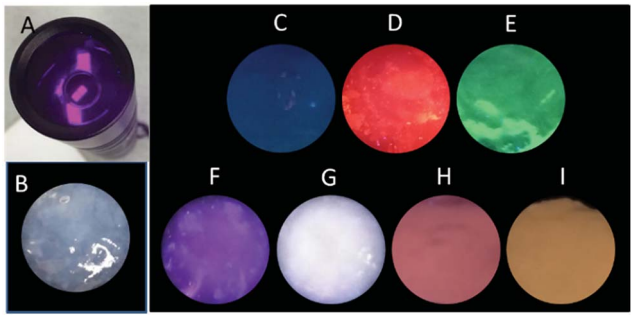

Fig. 7 (A) UV torch with excitation at 275 nm. (B) The photo of MOF gels coated on the torch under sunlight. The emission of MOF gels coated on the torch with different types and ratios of Ln^{3+} ion of (C) Dy, (D) Eu/Tb of 1 : 1, (E) Tb/Dy of 1 : 1, (F) Eu/Dy of 1 : 1, (G) Eu/Tb/Dy of 1 : 1 : 2, (H) Eu/Tb/Dy of 2 : 1 : 1, (I) Eu/Tb/Dy of 1 : 2 : 1 after the torch was lit.

Light-emitting diodes (LEDs) are the next generation of lighting systems by virtue of their environmental friendliness, high efficiency, and long lifetime.[38,39] White-emitting LED devices have been prepared by coating MOFs onto a UV lamp.[38,39] Our MOF gels were also coated onto a UV torch to reveal their UV-white emission transfer (Fig. 7). A white-emitting MOF gel was obtained with the ratio of Eu/Tb/Dy as 1 : 1 : 2, whereas colorful emissions were easily obtained from mixed-metal MOF gels (Fig. 7).

Multi-target detection with single MOF gels at single-wavelength excitation

A multi-target assay is achieved in a single matrix and attracts much interest.[40–42] Molecules were incorporated with multiple signal units such as electrochemiluminescence, fluorescence, and absorbance for multi-target sensing.[40] Light scattering signal, short-lived fluorescence, and long-lived phosphorescence from Mn-doped ZnS quantum dots (QDs) were used to discriminate proteins.[41] The "Lab-on-GO" system was built for protein assays with the catalysis, fluorescence, and assembly behavior of graphene oxide (GO).[42] However, different instruments are required for various signals and detection conditions are not well correlated. Herein, we propose that white-emitting MOF gels can be used for multi-target fluorescence detection at single-wavelength excitation. Fluorescence profiles of the white-emission MOF gels after addition of different targets are illustrated in Fig. S14.† The results in Fig. S15† revealed the multi-target detection of the white-emitting gels. A single signal with single-wavelength excitation led our system to a higher integration degree and simpler sensing procedure than the previous multi-target detection ones.[40–42]

Conclusions

MOFs are always considered as rigid materials, whereas gels are composed of soft and flexible three-dimensional cross-linked networks. Thus, it is sometimes difficult to conjugate MOFs to gels, but we reported a series of single- or mixed-Ln-MOF gels.

For the first time, the gels are equipped with intrinsic fluorescence emission. Moreover, the emission color is easily tuned by the simple selection of the type and ratio of Ln^{3+} ions for colorful emission under single-wavelength excitation. The formation mechanism of the gels was also thoroughly studied. The unique nucleation-growth mechanism revealed that the precursors first assembled to form nanoribbons, which then entangle to convert into MOF gels. The nanoribbons are formed through chemical bonds between the ligand and the metal ions, which is the essential property of chemical gels; the nanoribbons entangle through non-covalent interaction similar to that observed for physical gels. Therefore, MOF gels are chemical/physical hybrid gels. Our MOF gels represent the first example of MOFs that show viscoelastic properties and are the first gels to possess intrinsic fluorescence emission. The results of this study provide a new insight into the design of flexible MOFs and emissive gels for extensive applications in the near future.

Conflicts of interest

There are no conflicts to declare.

Acknowledgements

This work was supported by the Natural Science Foundation of China (No. 21435001, 21675090, and 21874074) and the National Basic Research Program of China (973 Program, No. 2015CB932001).

Notes and references

1 L. E. Buerkle and S. J. Rowan, *Chem. Soc. Rev.*, 2012, **41**, 6089–6102.
2 Q. Huang, Y. Zou, M. C. Arno, S. Chen, T. Wang, J. Gao, A. P. Dove and J. Du, *Chem. Soc. Rev.*, 2017, **46**, 6255–6275.
3 C. D. Jones and J. W. Steed, *Chem. Soc. Rev.*, 2016, **45**, 6546–6596.
4 H. Shibata, Y. J. Heo, T. Okitsu, Y. Matsunaga, T. Kawanishi and S. Takeuchi, *Proc. Natl. Acad. Sci. U. S. A.*, 2010, **107**, 17894–17898.
5 F. T. Moutos, L. E. Freed and F. Guilak, *Nat. Mater.*, 2007, **6**, 162–167.
6 Y. Luo, K. R. Kirker and G. D. Prestwich, *J. Controlled Release*, 2000, **69**, 169–184.
7 A. V. Salvekar, W. M. Huang, R. Xiao, Y. S. Wong, S. S. Venkatraman, K. H. Tay and Z. X. Shen, *Acc. Chem. Res.*, 2017, **50**, 141–150.
8 M. D. Konieczynska and M. W. Grinstaff, *Acc. Chem. Res.*, 2017, **50**, 151–160.
9 J. S. Kahn, Y. Hu and I. Willner, *Acc. Chem. Res.*, 2017, **50**, 680–690.
10 H. R. Culver, J. R. Clegg and N. A. Peppas, *Acc. Chem. Res.*, 2017, **50**, 170–178.
11 D. M. Zurcher, Y. J. Adhia, J. D. Romero and A. J. McNeil, *Chem. Commun.*, 2014, **50**, 7813–7816.
12 D. Nakayama, Y. Takeoka, M. Watanabe and K. Kataoka, *Angew. Chem., Int. Ed.*, 2003, **42**, 4197–4200.
13 H. J. Kim, J. H. Lee and M. Lee, *Angew. Chem., Int. Ed.*, 2005, **44**, 5810–5814.
14 K. Miyamae, M. Nakahata, Y. Takashima and A. Harada, *Angew. Chem., Int. Ed.*, 2015, **54**, 8984–8987.
15 M. M. Zhang, D. H. Xu, X. Z. Yan, J. Z. Chen, S. Y. Dong, B. Zheng and F. H. Huang, *Angew. Chem., Int. Ed.*, 2012, **51**, 7011–7015.
16 M. Zhou, J. Guo and C. Yang, *Sens. Actuators, B*, 2018, **264**, 52–58.
17 Q. Zhu, L. Zhang, K. Van Vliet, A. Miserez and N. Holten-Andersen, *ACS Appl. Mater. Interfaces*, 2018, **10**, 10409–10418.
18 H. Furukawa, K. E. Cordova, M. O'Keeffe and O. M. Yaghi, *Science*, 2013, **341**, 1230444.
19 L. Li, S. Xiang, S. Cao, J. Zhang, G. Ouyang, L. Chen and C.-Y. Su, *Nat. Commun.*, 2013, **4**, 1774.
20 A. K. Chaudhari and J.-C. Tan, *Chem. Commun.*, 2017, **53**, 8502–8505.
21 W. J. Gee and S. R. Batten, *Chem. Commun.*, 2012, **48**, 4830–4832.
22 M. R. Lohe, M. Rose and S. Kaskel, *Chem. Commun.*, 2009, 6056–6058.
23 J. S. Xiao, S. Y. Chen, J. Yi, H. F. Zhang and G. A. Ameer, *Adv. Funct. Mater.*, 2017, **27**, 1604872.
24 Y.-R. Liu, L. He, J. Zhang, X. Wang and C.-Y. Su, *Chem. Mater.*, 2009, **21**, 557–563.
25 T. Rodenas, I. Luz, G. Prieto, B. Seoane, H. Miro, A. Corma, F. Kapteijn, F. X. Llabrés i Xamena and J. Gascon, *Nat. Mater.*, 2015, **14**, 48–55.
26 B. Bueken, N. Van Velthoven, T. Willhammar, T. Stassin, I. Stassen, D. A. Keen, G. V. Baron, J. F. M. Denayer, R. Ameloot, S. Bals, D. De Vos and T. D. Bennett, *Chem. Sci.*, 2017, **8**, 3939–3948.
27 Y.-M. Wang, W. Liu and X.-B. Yin, *Chem. Sci.*, 2017, **8**, 3891–3897.
28 Y.-M. Wang, W. Liu and X.-B. Yin, *Adv. Funct. Mater.*, 2016, **26**, 8463–8470.
29 Z.-R. Yang, M.-M. Wang, X.-S. Wang and X.-B. Yin, *Anal. Chem.*, 2017, **89**, 1930–1936.
30 Y. J. Cui, B. L. Chen and G. D. Qian, *Coord. Chem. Rev.*, 2014, **273**, 76–86.
31 H. Xu, C.-S. Cao, X.-M. Kang and B. Zhao, *Dalton Trans.*, 2016, **45**, 18003–18017.
32 S. Freslon, Y. Luo, C. Daiguebonne, G. Calvez, K. Bernot and O. Guillou, *Inorg. Chem.*, 2016, **55**, 794–802.
33 H. Deng, C. J. Doonan, H. Furukawa, R. B. Ferreira, J. Towne, C. B. Knobler, B. Wang and O. M. Yaghi, *Science*, 2010, **327**, 846–850.
34 X. Rao, T. Song, J. Gao, Y. Cui, Y. Yang, C. Wu, B. Chen and G. A. Qian, *J. Am. Chem. Soc.*, 2013, **135**, 15559–15564.
35 Y. Wen, T. Sheng, X. Zhu, C. Zhuo, S. Su, H. Li, S. Hu, Q.-L. Zhu and X. Wu, *Adv. Mater.*, 2017, **29**, 1700778.
36 Y. J. Cui, T. Song, J. C. Yu, Y. Yang, Z. Y. Wang and G. D. Qian, *Adv. Funct. Mater.*, 2015, **25**, 4796–4802.

37 Y. Lu and B. Yan, *Chem. Commun.*, 2014, **50**, 15443–15446.
38 Y. Cui, T. Song, J. Yu, Y. Yang, Z. Wang and G. Qian, *Adv. Funct. Mater.*, 2015, **25**, 4796–4802.
39 Y. W. Zhao, F. Q. Zhang and X. M. Zhang, *ACS Appl. Mater. Interfaces*, 2016, **8**, 24123–24130.
40 K. Chen, Q. H. Shu and M. Schmittel, *Chem. Soc. Rev.*, 2015, **44**, 136–160.
41 P. Wu, L. N. Miao, H. F. Wang, X. G. Shao and X. P. A. Yan, *Angew. Chem., Int. Ed.*, 2011, **50**, 8118–8121.
42 Y. X. Lu, H. Kong, F. Wen, S. C. Zhang and X. R. Zhang, *Chem. Commun.*, 2013, **49**, 81–83.